Available online at www.sciencedirect.com
SCIENCE DIRECT®
Polymer 44 (2003) 5915–5925
polymer
www.elsevier.com/locate/polymer

Observations of structure development during crystallisation of oriented poly(ethylene terephthalate)

A. Mahendrasingam[a,*], D.J. Blundell[a], A.K. Wright[a], V. Urban[b], T. Narayanan[b], W. Fuller[a]

[a]*School of Chemistry and Physics, Keele University, Staffordshire ST5 5BG, UK*
[b]*ESRF, BP 220, F-38043 Grenoble Cedex, France*

Received 31 January 2003; received in revised form 14 May 2003; accepted 14 May 2003

Dedicated to Prof. Ian M. Ward on the occasion of his 75th birthday

Abstract

Two types of SAXS and WAXS experiments have been made using synchrotron radiation to observe the transformation from smectic to crystalline phases in oriented poly(ethylene terephthalate) (PET). In step-anneal experiments, PET was drawn slowly at 30 °C and then observed after annealing at 5 °C steps up to 100 °C. In the other experiments, time-resolved observations were made while drawing at 90 °C at rates up to 10 s^{-1}. Up to 70 °C the WAXS data in the step-anneal experiments showed the smectic meridional reflection reducing in lateral width, indicating an increase in lateral long range order with annealing. Between 70 and 100 °C, there was a reduction in the intensity of the smectic reflection which correlated with an increase in the intensity of crystalline reflections. The SAXS from the step-anneal experiments showed an intense equatorial streak which has a correlation peak around 20 nm and which diminishes with annealing above 70 °C. It is concluded that this feature is a characteristic of the presence of the mesophase in oriented PET and is due to elongated domains of smectic mesophase with a length >75 nm and with an interdomain spacing of around 20 nm. Between 70 and 100 °C the SAXS data showed additional diffuse diffraction which correlated quantitatively with the crystalline phase and evolved from a cross-like appearance to a well resolved four-point pattern. The time-resolved drawing experiments were limited by the time resolution of the SAXS detector. They showed the same development of four-point diffuse SAXS patterns as was observed in the step-anneal experiments and a very weak equatorial streak. Differences in phase transformation kinetics between the two types of experiment are attributed to the different chain relaxation processes available under different conditions.

Keywords: Poly(ethylene terephthalate); Mesophase; Crystallization

1. Introduction

Oriented poly(ethylene terephthalate) (PET) is used extensively in the manufacture of films, bottles and fibres. The enhanced properties resulting from high orientation rely on crystallisation 'fixing' the chain orientation and providing dimensional stability. This paper is a continuation of our previous studies of oriented PET [1,2]. It reports on observations from recent synchrotron WAXS and SAXS experiments of the development of crystallinity via pre-crystalline structures. The observations of pre-crystalline structure are also relevant to the current general debate on the role of an intermediate mesophase acting as precursor of the crystalline phase during polymer crystallization [3–6].

In a previous paper, we have reported a time-resolved WAXS synchrotron study of the strain-induced crystallisation process during the orientation of PET [7], in which a transient, smectic mesophase was seen to be created during drawing before being transformed into an oriented crystalline phase. The mesophase is characterised by a sharp meridional reflection at ~1.03 nm and by diffuse equatorial diffraction lobes. The diffuse equatorial diffraction is consistent with the parallel alignment of chains packed in a liquid like manner. The meridional spacing is smaller than the *c*-axis repeat of the triclinic crystal phase (1.075 nm) and has been shown to be consistent with a random chain conformation with CO–O–C–C dihedral angles close to 80° [8,9]. The meridional reflection has a narrow lateral spread which indicates a degree of correlated registration

* Corresponding author. Tel.: +44-1782-583312; fax: +44-1782-583320.
E-mail address: a.mahendrasingam@keele.ac.uk (A. Mahendrasingam).

0032-3861/03/$ - see front matter © 2003 Published by Elsevier Ltd.
doi:10.1016/S0032-3861(03)00542-1

between monomers of adjacent chains such that the plane of registration is perpendicular to the chain direction. This differs from the triclinic crystal structure of PET where the plane of registration of monomer units is on a slant with respect to the chain direction. Such a correlation between monomer segments of aligned chains has been termed a 'chained smectic' structure [10]. A diffraction pattern with diffuse equatorial lobes but without this meridional feature would indicate a lack of correlated registration between units of adjacent chains such that the arrangement of monomer units would be characteristic of a nematic phase.

In a separate study, Welsh et al. [11,12] have shown evidence of the smectic mesophase occurring as a transient state in the oriented crystallisation of a range of poly-(ethylene terephthalate)/poly(ethylene 2,6 naphthalate) (PET/PEN) copolymers. An associated real time study of the deformation of a 50% PET/50% PEN copolymer demonstrated that in the absence of crystallisation the smectic mesophase can attain a degree of self-stability which resists decay from chain relaxation processes, thus supporting the view that this mesophase represents a thermodynamic state [13].

There have been several reports of a mesophase occurring in oriented PET when prepared under specific conditions. Bonart [14] recognised both nematic and smectic states in a series of stretching experiments on PET and originally suggested that these mesophase states characterise stages in the crystallisation process. Later Bonart carried out cold drawing under various conditions and claimed to be able to produce all-nematic or all-smectic forms [15]. Asano and Seto [16] observed similar patterns in cold drawn and annealed fibres. Recently Asano et al. [17] have expanded the study on cold drawn PET that is subsequently annealed and demonstrated with increasing temperature a progression from nematic to smectic and from smectic to crystalline order. There have also been speculations of the smectic state influencing the orientation texture of the subsequent crystals such as the tilt of the chain axis away from the draw direction [12,17].

In the case of unoriented PET, Imai and coworkers [18] have presented clear evidence from SAXS of density fluctuations developing via a spinodal process which they have interpreted as precursors to the crystal nucleation process. Olmsted et al. [5] have rationalised the formation of an intermediate mesophase via a spinodal process in terms of an assisted crystallisation model involving a buried liquid–liquid phase. There is therefore an impetus to integrate SAXS information with WAXS data in order to elucidate the evolution of the crystalline structure that is specific to oriented PET.

The majority of previous SAXS studies of oriented PET have been based on the post analysis of previously oriented and crystallised samples. In most cases the SAXS patterns of uniaxially oriented PET exhibit a four-point pattern of diffraction maxima. Explanations of the origin of the four-point pattern include a checker-board arrangement of crystallites and lamellar like crystals with sloping end surfaces [19].

This paper describes two types of real time X-ray scattering experiments that have been carried out on oriented crystallisation of PET using a synchrotron source. The first type involves time-resolved SAXS observations during fast, uniaxial deformation. These experiments were carried out under the same conditions as used in our previous WAXS studies [1,2]. These studies used strain rates up to $\sim 10\ s^{-1}$ in order to simulate conditions used in many industrial film and bottle fabrication processes. The studies identified two main regimes of behaviour which depended on the drawing conditions and which correlated with the chain relaxation modes. In regime I, when the deformation rate was faster than chain retraction modes, it was found that the onset of crystallisation was delayed until the end of the deformation process, irrespective of the draw ratio achieved. However, in regime II, when the strain rate was slower than chain retraction, crystallisation started to occur during the deformation process once sufficient chain segment orientation had been achieved. However, these experiments were only able to resolve the meridional smectic reflection while drawing at the lowest temperature (90 °C) and fastest strain rate of $10\ s^{-1}$ [7]. It is not known whether this is due to limited resolution or because the smectic reflections only occur under limited conditions. All these previous WAXS observations were made using a CCD camera and frame grabber configuration that enabled the recording of successive frames every 40 ms. This provided the time resolution that was needed to record the events occurring during the fastest draw rates. The new SAXS experiments reported here were carried out at the ESRF in Grenoble on beamline ID2A, since this was regarded as the facility which has the most appropriate configuration for the continuous time resolution of SAXS and which therefore was most able to capture these faint transient diffraction effects. However the configuration of the CCD on this beamline has a dump time between frames of 0.1 s and thus precludes resolution of the fastest draw rates. Nevertheless it is still adequate for resolving the slower draw rates of regime I conditions at 90 °C.

The second type of experiment attempted to reproduce the experiments of Asano et al. [17] in which the PET is slowly cold drawn and is then progressively annealed at 5 °C increments during which there is a gradual ordering of structure resulting in oriented crystallisation. WAXS and SAXS diffraction were recorded in two separate experiments using the same procedure. Although this experiment does not fully simulate events occurring during the time-resolved fast drawing experiments, it has the advantage of not being limited by time resolution and hence provides useful insight into the structure evolution.

The main objectives of this work are to look for evidence in the SAXS of density fluctuations that correlate with the smectic meridional reflection and to follow the evolution of the four-point pattern during the build up of the crystalline

phase. It will be shown that the smectic phase gives rise to equatorial diffraction lobes indicating a columnar-like morphology.

2. Experimental

Experimental data were collected at the ESRF in Grenoble using X-rays of wavelength 0.095 nm on beamline ID2A. The SAXS patterns were collected on a CCD with a sample to detector distance of 2.5 m. Variations in beam intensity before and after the sample were monitored in real time with pin diodes. The ratio of the two readings enabled corrections to be made for sample absorption in order to obtain appropriate subtraction of the background signal. During the SAXS experiments, a second CCD was positioned at an oblique angle at a distance of around 150 mm to enable the part of the WAXS diffraction on the equator to be recorded simultaneously with the SAXS pattern. This subsidiary WAXS pattern allowed the crystallisation process to be correlated with the changing SAXS patterns. Full WAXS patterns were recorded in separate experiments using a Photonics Science CCD with a specimen-detector distance of 60 mm in order accurately to record the meridional reflection associated with the smectic phase.

All the deformation experiments were carried out in situ with the samples mounted in the jaws of a stretching X-ray camera that had been purpose designed and constructed in the Keele Physics Department workshops [20,21]. The temperature of the oven could be controlled to within 1 °C. The jaws of the camera were attached to stepper motors which allowed uniaxial, bi-directional drawing allowing effective strain rates up to $\sim 10\ s^{-1}$.

The PET polymer was supplied by Goodfellow and was in the form of an amorphous sheet of thickness 1 mm. Specimens 10 mm wide were cut from a sheet and ink reference stripes were drawn with a separation of 1 mm on the specimen at right angles to the draw direction to enable the degree of extension to be deduced from the video camera image. The specimen was mounted in the jaws of the camera with a 10 mm gauge length.

For the real-time SAXS drawing experiments, the specimens were heated in the camera to the drawing temperature and allowed to equilibrate for 2 min before being drawn. They were then drawn to the final draw ratio of around 3.5:1 by stepping the motors with pre-defined steps. A sequence of 0.1 s SAXS frames were collected every 0.12 s over the time scale of the experiments. The drawing experiments were carried out at 90 °C at various deformation rates between 0.1 and $10\ s^{-1}$.

For the slow drawing and step-annealing experiments, the specimens were first drawn at 30 °C at a deformation rate of $10^{-3}\ s^{-1}$ to a final draw ratio of $\sim$3.5:1. The temperature was then raised in 5 °C steps to 100 °C with diffraction patterns being recorded over 10 s at each temperature while the sample was firmly held in the jaws of the stretching rig. One set of data recorded the full WAXS pattern using the Photonics CCD at 60 mm and a second separate experiment recorded the SAXS patterns with the CCD at 2.5 m path length.

Before analysis of the patterns, the background scatter with an empty camera was subtracted taking account of the transmission factor determined from the pin diode signal on the backstop. Estimates of the invariant integral from the SAXS patterns were obtained by assuming the intensity function had uniaxial symmetry around the draw axis. The two-dimensional pattern was projected on to the equatorial axis to obtain a one dimensional intensity profile $J(s)$, where s is the scattering vector defined by $s = 2 \sin \theta/\lambda$. Since the signal to noise of the pattern did not allow the high-s part of the profile to be analysed in detail, it was assumed for simplicity that the decay of the $J(s)$ profile had a $1/s^3$ dependence. A constant background value, B, due to random density fluctuations, was therefore chosen for subtraction from $J(s)$ so as to give the $1/s^3$ dependence. The invariant, Inv, was then calculated from a summation based on

$$\mathrm{Inv} = 2\pi \int_0^\infty (J(s) - B)s\, \mathrm{d}s \tag{1}$$

where $J(s)$ was calibrated in absolute units from a secondary intensity standard.

The development of crystallinity and orientation was obtained from macro programs using the methods developed previously [1,2,22]. Estimates of crystallinity were obtained from radial scans of the WAXS patterns by fitting a Pearson VII function to crystalline reflections [2]. Information on orientation before the onset of crystallisation was obtained from azimuthal circular scans around the amorphous halo at a reciprocal space vector of $0.028\ nm^{-1}$. The profile was used to calculate an orientation order parameter $P_2(\cos \phi)$ where ϕ is the angle between the chain axis and draw direction [1].

3. Results

3.1. Real-time drawing experiments

An example of the results from the real time drawing experiments is shown in Fig. 1 which illustrates selected SAXS patterns from the experiment carried out at 90 °C at a strain rate of $1\ s^{-1}$ and a final draw ratio of 3.3:1. Fig. 2 shows the simultaneous WAXS pattern in the region of the equator. In this experiment, frame 1 shows the initial pattern of the undeformed sample. Frame 8 is near to the end of the deformation. The frames between 9 and 49 show patterns after the deformation process while the sample is at its final length.

There are two main features in the SAXS patterns: an intense diffraction close to the beam stop and diffuse

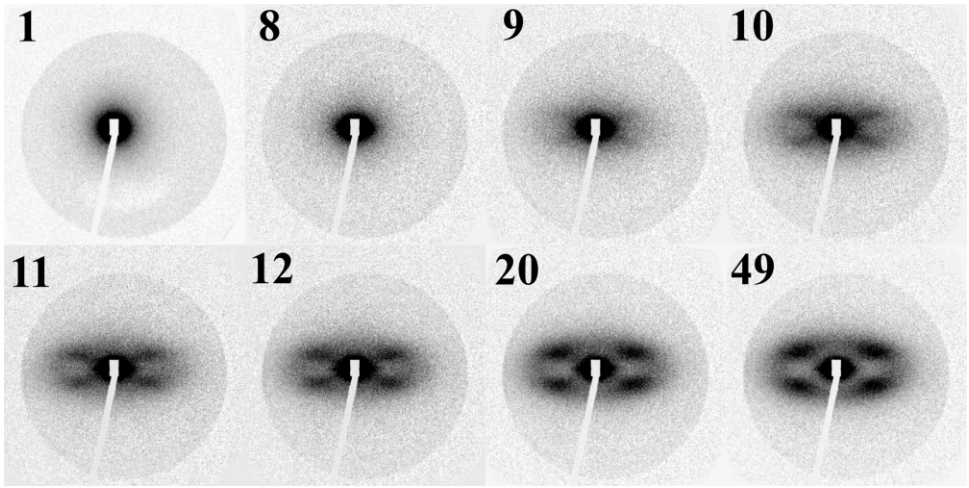

Fig. 1. Selected SAXS frames from the time-resolved drawing experiment at 90 °C and 1 s^{-1}, where frames were collected in 0.12 s intervals. Frame 1 undrawn sample. Frame 8 is near the end of deformation process. Frames 9, 10, 11,12, 20 and 49 at fixed length after deformation.

diffraction at higher scattering angles. The intense central scatter is initially isotropic. During the deformation, a second component in the form of a weak, narrow equatorial streak is superimposed on the intense central feature. Diffuse diffraction at higher angles could not be detected during the deformation phase between frames 1 and 8. However, a clear diffuse pattern develops with 4-point maxima between frames 9 and 49 after the deformation. During this time there are small, significant changes in the 4-point pattern. In the early stage in frame 9, the pattern is closer to the main beam and gives the appearance of a diagonal cross. The WAXS patterns in Fig. 2 show the development of crystalline diffraction spots between frames 9 and 49. These spots correlate closely with the appearance of the four-point SAXS pattern. Experiments which were carried out at other draw rates show SAXS patterns with the same features at corresponding stages in the experiment. However the time resolution of the effects becomes progressively poorer at the faster draw rates.

In these experiments, as well as our previously reported WAXS experiments, no meridional smectic diffraction could be resolved at strain rates below 10 s^{-1}. Unfortunately, for the highest strain rate of 10 s^{-1}, there was not sufficient time resolution in the current SAXS experiments to capture any effects associated with the previously reported, transient, mesophase at the onset of crystallisation [7].

3.2. Step-annealing experiments

Fig. 3 shows the WAXS patterns at selected temperatures from the step-annealing experiments. The smectic meridional reflection is highlighted as an insert. Fig. 4 shows corresponding frames from the associated SAXS experiment carried out under identical conditions.

The WAXS patterns correspond well with the effects seen in the study by Asano et al. [17]. One exception is that at the lowest annealing temperature of 35 °C a faint smectic reflection can be discerned, whereas Asano et al. report its complete absence. This could be due to our cold drawing being carried out at a higher temperature and faster draw rate than used by Asano et al. Up to 70 °C the equatorial diffraction remains unchanged in the form of a diffuse spot, indicating well aligned chains without crystallographic register. Azimuthal scans through the equatorial diffuse scatter indicate that the $P_2(\cos\phi)$ orientation parameter between 35 and 65 °C has a value close to 0.65. This is significantly larger than was found in previous time-resolved drawing experiments [1]. For example, while drawing at 90 °C, $P_2(\cos\phi)$ at the end of the draw was

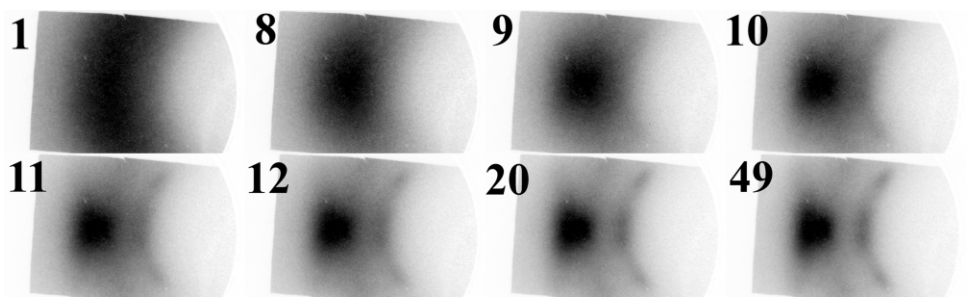

Fig. 2. Selected WAXS frames from the time-resolved drawing experiment at 90 °C and 1 s^{-1}, where frames were collected in 0.12 s intervals. Frame 8 is near the end of deformation process. Frames 9, 10, 11, 12, 20 and 49 at fixed length after deformation.

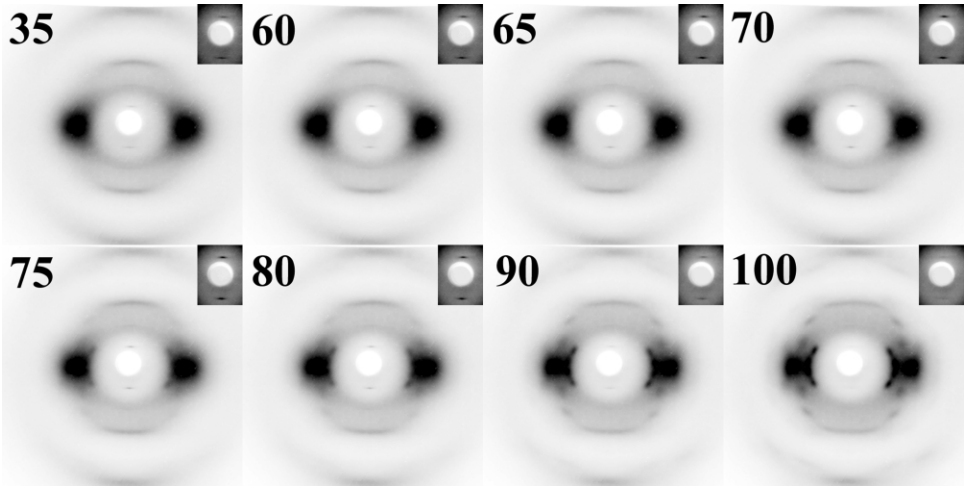

Fig. 3. Selected WAXS full patterns from step-anneal experiment after annealing at 35, 60, 65, 70, 75, 80, 90 and 100 °C. The inserts in the top right hand corner show the central region containing the smectic meridional reflection.

previously found to have reached values of 0.47 and 0.23 with strain rates of 10 and 1 s^{-1}, respectively. When the temperature reaches 70 °C, the meridional reflection increases in visibility but crystalline reflections are appearing within the equatorial diffuse diffraction. Between 70 and 100 °C, the crystalline reflections become stronger while there is a corresponding wane in the meridional smectic reflection. At 100 °C the smectic reflection is no longer visible.

The SAXS patterns in Fig. 4 are broadly similar to those in the time-resolved drawing experiments and show central scatter near the beamstop as well as higher angle diffuse patterns. The central scatter consists of an isotropic component and an equatorial streak. However, the equatorial streak is more pronounced than in the time-resolved data in Fig. 1. Scans along the equator are shown in Fig. 5 at selected temperatures. At 35 °C, the diffraction profile appears to have a broad shoulder suggesting a structure to the scattering. The lateral spread of the scattering curve becomes sharper with increasing temperature and the profiles appear to converge beyond 90 °C, due to a weakening of the equatorial streak. Fig. 6 shows a comparison of the 100 °C scan with equatorial scans from some of the patterns from the fast draw experiment. Significantly, these scans include the isotropic undrawn sample as well as the fully drawn, crystallised sample. Each of the scans from the fast draw experiment have been rescaled in order to compensate for intensity differences due to differences in orientation and scattering power. It will be noted that after rescaling, these monotonic scattering profiles are all identical within experimental error. The fact that one of these scans is from the unoriented sample indicates that this monotonic scatter is mainly due to the isotropic component with very little contribution from the equatorial streak. It is therefore reasonable to regard the isotropic scatter as a spurious feature that is not related to the development of oriented structure of the polymer. One possibility is that it is caused by particulate additives from the manufacturing process of this material. More importantly, one can conclude that the equatorial streak can be

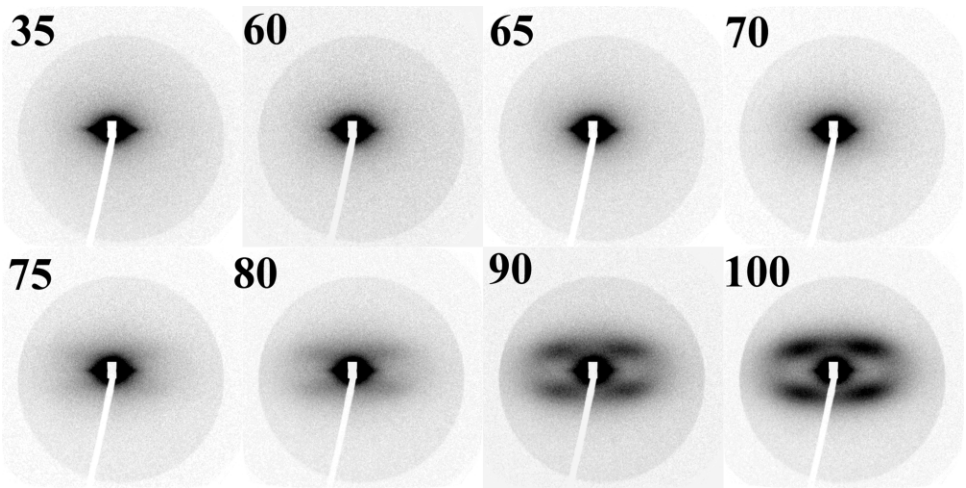

Fig. 4. Selected SAXS full patterns from step-anneal experiment after annealing at 35, 60, 65, 70, 75, 80, 90 and 100 °C.

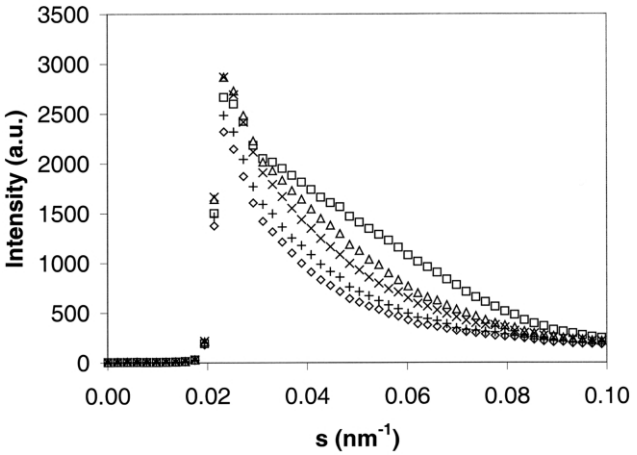

Fig. 5. Equatorial scans from SAXS of Fig. 4 for the step-anneal experiment. (□) 35 °C; (△); 65 °C; (×) 75 °C; (+) 85 °C; (◇) 100 °C.

attributed to a structure in the polymer that is introduced by the cold drawing process. Fig. 7 shows the result of subtracting the profile at 100 °C from the profiles at lower temperatures in order to extract the contribution from the equatorial streak. The resulting diffraction profiles now show clear correlation peaks corresponding to Bragg spacings of 19 nm at 35 °C increasing to around 24 nm at 80 °C. Some corresponding subtractions of the 100 °C two-dimensional patterns are shown in Fig. 8. These patterns clearly show the nature and the changes of the equatorial streak as a function of temperature. Vertical scans through the equatorial streak show a meridional width of around 0.013 nm^{-1} which indicates that the structure causing the scatter has a vertical spread of at least 75 nm.

At larger scattering angles beyond the central region of the beamstop, there is no discernable SAXS diffraction at temperatures below 70 °C. Above 70 °C, a four-point diffuse pattern develops in prominence and correlates closely with the developing crystallinity. The earliest appearance of this diffuse pattern at 70 °C is more compact and resembles the

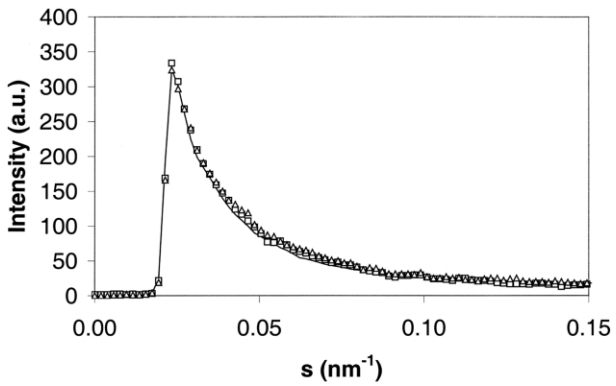

Fig. 6. Comparison of equatorial scans demonstrating similarity of profile between step-anneal and time-resolved experiment. (□) undrawn sample in time-resolved experiment; (△) end of draw in time-resolved experiment; (line) step-anneal experiment at 100 °C.

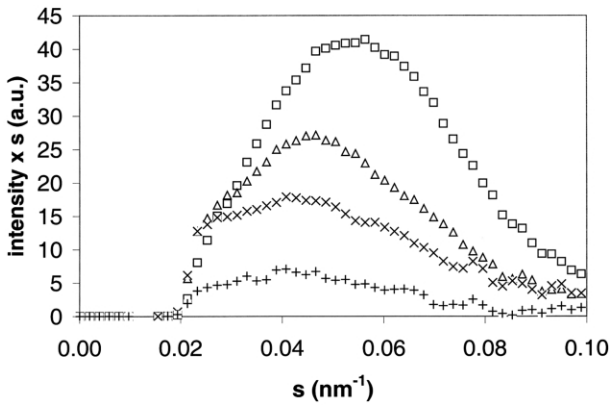

Fig. 7. SAXS equatorial scans from Fig. 4 after subtraction of profile for 100 °C. An axial Lorentz correction has been applied to the SAXS data. (□) 35 °C; (△) 65 °C; (×) 75 °C; (+) 85 °C.

diagonal cross pattern in frame 9 of Fig. 1 for the real time drawing experiment.

4. Discussion

4.1. Development of smectic structure

The overall observations from the step-anneal experiment agree well with the work of previous authors, in particular that of Asano et al. [17]. The meridional reflection from the smectic state reaches a maximum in prominence at around 70 °C and thereafter diminishes and becomes unresolvable at 100 °C. Along with this, discrete reflections from the triclinic crystalline phase become resolvable at 70 °C and grow in strength. The present experiments however do show some differences as well as some additional information.

One of the differences is that the smectic meridional reflection is already faintly visible in the ‘as-drawn’ state at 30 °C. Asano et al. were unable to resolve this reflection and therefore classed their starting material as effectively nematic in nature with no longitudinal correlation between neighbouring chains. In order to clarify this situation, we made scans laterally across the whole meridional reflection using a scanning width that fully encompassed the meridional spread of the reflection. The resulting intensity profiles were analysed by fitting the peaks with a Pearson VII function. Fig. 9 shows the peak height and lateral width at half height of the fitted profiles. The data show an increase in peak height up to 70 °C but also a compensating narrowing of the lateral width of the reflection. In order to assess the total intensity associated with the smectic reflection one needs to integrate the intensity function over the three dimensions of reciprocal space. It is necessary to recognise that the observed diffraction patterns are related to the intersection of the three-dimensional intensity function by the two-dimensional surface of the Ewald sphere. On the assumption that the structure of the sample

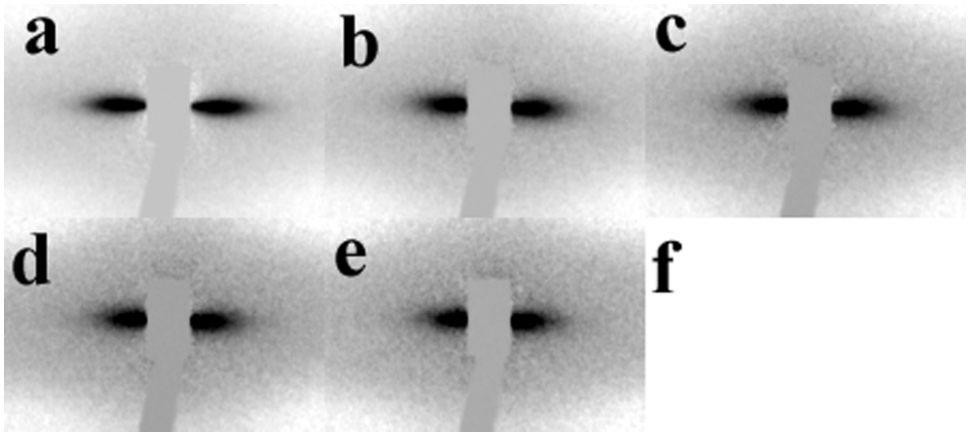

Fig. 8. Result of subtracting the SAXS pattern at 100 °C from selected lower temperature patterns of the step-anneal experiment showing the central scatter near the beamstop. (a) 35 °C, (b) 65 °C, (c) 70 °C, (d) 75 °C, (e) 80 °C, (f) 100 °C.

has uniaxial symmetry, the total intensity can therefore be estimated by multiplying the peak height by the square of the lateral peak width. As is shown in Fig. 9, the resulting integrated intensity shows a barely significant decrease up to 70 °C followed by a steep fall to zero at 100 °C. The decrease in lateral width between 30 and 70 °C can be visualised either as an increase in the size of domains of smectic order or as an improvement in longitudinal register increasing the range of lateral correlation of smectic order. The slight fall in total intensity up to 70 °C suggests that the improvement in lateral coherence of smectic order is gained at the expense of the overall amount of smectic mesophase. An analysis of the lateral peak width using the Scherrer relationship indicates an increase in lateral coherence or domain size from 2 to 4 nm, which is equivalent to an increase from about 5 to 8 chain widths. Therefore up to 70 °C, approximately the same number of chains are involved in a smectic type of structure but that there is a significant increase in the lateral range of smectic correlation. One therefore concludes that the lateral coherence of the smectic regions increases by a smooth

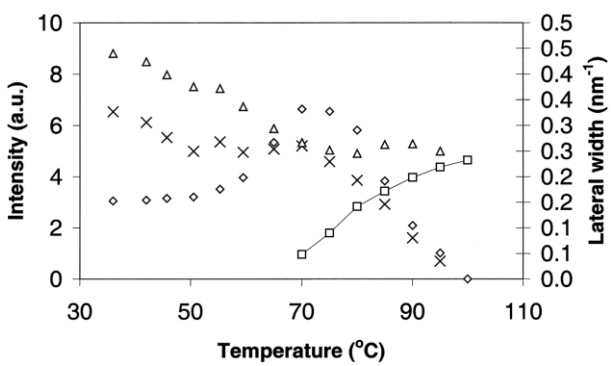

Fig. 9. Variation of WAXS reflections from the smectic and crystalline phases in the step-anneal experiment. (◇) peak height of smectic meridional reflection (a.u.); (△) lateral width of smectic reflection (nm^{-1}); (×) integrated intensity of smectic reflection (height × (lateral width)^2) (a.u.); (□) crystalline peak intensity (a.u.).

ripening process during annealing up to 70 °C. Scans through the smectic reflection in the meridional direction show that the half-width in this direction does not change with temperature. This measured half-width is close to the angular resolution of the beam configuration and is therefore insensitive to changes. On the basis of the Scherrer relationship, the merdional width indicates that the short range coherence of the smectic order in the chain direction is at least 15 nm.

The equatorial streak in the SAXS scatter shown in Fig. 8 occurs over the same temperature range as the smectic meridional WAXS reflection. This is a strong indication of a direct link between the smectic mesophase and the superstructure associated with the equatorial scatter. More information on the nature of this superstructure can be obtained from the absolute intensity of the equatorial streak shown in Fig. 7. An estimate was therefore made of the Invariant integral over the central region of the SAXS pattern using the relationship Eq. (1). In view of the very low intensity of this component, the calculation of the integral given in Eq. (1) was restricted to a limited range of s without a contribution from a $1/s^3$ tail. Since the excess scatter shown in Fig. 7 is already the result of the subtraction of two frames with the same background component, the background B was taken to be zero.

Estimates based on this calculation indicate that the Invariant integral decreases from 6×10^{-6} (mole electrons/cc)^2 at 35 °C to 4×10^{-6} (mole electrons/cc)^2 at 70 °C. Equatorial scatter in the form of a narrow streak can generally be attributed to either elongated microvoids formed as a result of the cold deformation process or to a density fluctuation from a needle-like phase structure. The former possibility can be shown to be unlikely by considering the scatter in terms of a two phase model in which the Invariant would be given by [19]:

$$\text{Inv} = \chi(1 - \chi)\Delta\rho_e^2 \tag{2}$$

where χ is the volume fraction of one of the phases and $\Delta\rho_e$

is the difference in electron density between the two phases. In the case of microvoids the electron density difference relative to PET would be about 0.7 mole electrons/cc. According to relationship Eq. (2), one would therefore predict that the voids account for a volume fraction of the order of 10^{-5}. If such voids are to be arranged so as to give a diffraction maxima with a correlation period equivalent to the observed 20 nm, then the dimensions of the voids would need to be about 2×10^{-4} nm. The concept of a void of this size is meaningless relative to the size of an atom and it is therefore reasonable to discount microvoids as the source of the scatter. If on the other hand one assumes that the scatter is due to density fluctuations, the two phase approximation of Eq. (2) can also be used to estimate the magnitude of the fluctuations. For a volume fraction of one of the two phases anywhere between 0.1 and 0.9, Eq. (2) predicts an electron density difference of around 0.005 mole electrons/cc or a mass density difference of around 0.01 g/cc. This is of the order of magnitude expected from an embedded mesophase. It is in fact close to the difference proposed by Asano and coworkers [17] between the density of the smectic mesophase (1.38) and the density of oriented amorphous PET (1.37). It is therefore plausible to attribute the equatorial streak to an intrinsic lateral density fluctuation resulting from the presence of the smectic mesophase.

Thus the equatorial SAXS suggests a needle-like or columnar superstructure comprising regions of oriented smectic order alternating with less ordered regions. The intensity distribution of the equatorial lobes indicate smectic domains which are at least 75 nm long in the draw direction and which are separated from each other by around 20 nm. The Scherrer analysis of the WAXS meridional reflection indicates that the lateral spatial coherence between chains in the smectic domains extends over 2–4 nm. One could therefore regard the SAXS equatorial lobes as the signature of the precursor smectic mesophase in oriented PET. It is debatable how this scatter can be related to the isotropic scatter associated with the precursor density fluctuations observed by Imai et al. [18] during the crystallization of unoriented PET.

It is a possibility that the formation of the needle-like superstructure in the oriented case can be attributed to the restricted molecular mobility at the low deformation temperature. The initial 30 °C drawing process in the step-anneal experiment occurs at 40 °C below the nominal T_g of PET. This will involve higher levels of internal stress and more severe restrictions on molecular motions compared with the time-resolved drawing experiments at 90 °C. Our previous time-resolved studies identified three regimes of crystallisation behaviour [1]. For regime I, covering strain rates from 1 to 10 s^{-1} at 90 °C (as in the present time-resolved experiments), the onset of crystallisation was found to be delayed until the end of the deformation process. An analysis of chain relaxation modes demonstrated that this could be attributed to the draw rate being faster than chain retraction motions. It was proposed that the oriented chains are unable to achieved crystallographic packing of the triclinic crystal cell without the ability to retract and slip through restraining entanglements. Under the conditions of draw at 30 °C in the step-anneal experiment, the hindrance to relaxation will be even more severe. The thermal activation of retraction motions would be effectively inoperative and even the basic Rouse relaxation modes would be expected to be severely restricted, if not inoperative within the timescale of the experiment. Only the faster localised motions of the relaxation spectrum would be available from thermal activation. The elongation of chains during plastic extension below T_g involves conformational changes by stress activated processes. In the absence of thermal activated chain relaxations, crystallisation of the elongated chains is not possible. However, the formation of the smectic phase is less demanding and does not require that the neighbouring chains have identical conformations and such precise register. It is therefore conceivable that smectic order can be achieved between neighbouring elongated chains by means of localised chain motions. The presence of smectic regions while deformation is still in progress could result in the formation of an inhomogeneous superstructure comprising more rigid regions which resist deformation and more mobile regions that provide the compliance for continued plastic flow. Such a flow induced segregation could be the origin of the needle-like superstructure associated with the SAXS equatorial scatter.

Motions associated with chain retraction would not become operative until the temperature is raised in the annealing stages of the experiment. Lower annealing temperatures would be expected to only allow localised chain motions to provide small adjustments to chain conformation and packing. This would explain the improvement in smectic order observed between 30 and 70 °C. Higher annealing temperatures would enable the chain retraction motions which on the basis of our previous reasoning would allow the smectic chains to re-position and stack in a crystallographic register.

It is worth noting that the 20 nm correlation distance is consistent with the structures previously observed by Prevorsek et al. [23] using electron microscopy of crystallised PET fibres. Prevorsek et al. interpreted the data as a matrix of extended non-crystalline chains in which there were embedded microfibrils of alternate crystalline and disordered chains. If their interpretation is relevant to the present data, it could imply that the smectic structure is associated with needle-like domains that are precursors of the proposed microfibrils.

Due to the current limitations of time resolution it was not possible to obtain SAXS data from real time drawing experiments at 90 °C at 10 s^{-1} which were the conditions where meridional reflection of the transient mesophase was observed in our previous experiments [7]. Further experiments are therefore planned to examine real time drawing using higher time resolution.

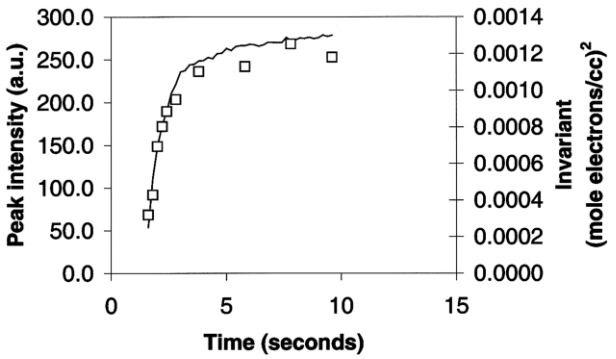

Fig. 10. Comparison of intensity of crystalline WAXS reflection with SAXS Invariant Integral for the time-resolved drawing experiment. (Line) crystalline reflection; (□) SAXS invariant.

4.2. Formation of crystal phase

The WAXS data from the step-anneal experiment substantiates the observations of our previous fast drawing experiments in providing further evidence of the mesophase being an intermediate precursor to crystallisation in which the crystalline phase forms at the expense of the smectic mesophase. This is clearly shown in Fig. 9 which compares the intensity of the crystalline reflections with the intensity of the smectic meridional reflection. The comparison of the intensities shows in a quantitative way the onset of the crystallisation coinciding with the start of the decrease in mesophase.

Both experiments also show a close correlation between the diffuse, four-point SAXS pattern and the discrete crystalline reflections in the WAXS patterns. Fig. 10 shows a comparisons of the SAXS invariant integral and the intensity of the crystalline reflections derived from the data shown in Fig. 1 for the fast drawing experiments. Fig. 11 shows a corresponding comparison for the step-anneal experiments derived from the patterns in Figs. 3 and 4. There are similar increases in both parameters. The absolute intensity of the diffuse SAXS component is also consistent with the crystalline phase. Using relationship [1], the

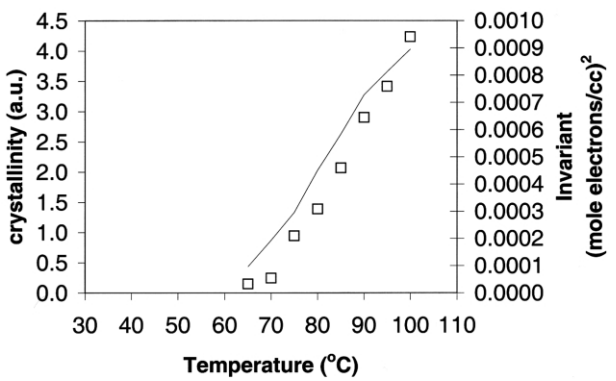

Fig. 11. Comparison of intensity of crystalline WAXS reflection with SAXS invariant integral for the step-anneal experiment. (Line) crystalline reflection; (□) SAXS invariant.

absolute SAXS invariant at 100 °C was estimated to be 9×10^{-4} (mole electron/cc)^2. According to Asano et al., the crystallinity after annealing at 100 °C will be around 22%. Using this value in the two phase approximation of relationship [2], the invariant would accordingly indicate an electron density difference of ~0.07 mole electrons/cc; i.e. an absolute density difference of ~0.14 g/cc. This is of the order expected for the difference between the densities [24] of the crystalline (1.455 g/cc) and amorphous (1.335 g/cc) phases and is a further indication that the four-point SAXS pattern is associated with the crystal phase and is not associated with a mesophase precursor. This differs from the view of Asano et al. [17] who propose that the earliest diffuse SAXS scatter is attributable to a precursor state before the appearance of crystallinity.

4.3. Kinetics of smectic-crystal transformation

Although both the step-anneal and the time-resolved fast drawing experiments provide evidence of the smectic phase occurring as a precursor to the crystalline state, there is a clear difference in the transformation process. In the step-anneal experiments, both phases have a stable coexistence for times in excess of 10 min over the temperature range 70–95 °C. In contrast, in our previous fast drawing experiments at a constant 90 °C, the smectic exists as a transient which fully transforms to the crystal within about 0.25 s [7]. There is clearly a difference in the stability of the smectic phase which must relate to the history of the two types of sample. The kinetics of the full transformation from oriented disordered chains to smectic state to crystalline state are not understood and will vary according to the conditions and restraints of each situation, including differences in the degree of chain orientation. The size of a smectic domain and the degree of imposed constraint could also affect the stability of the domain and hence its lifetime as an intermediate state. This difference between the experiments may be a consequence of different regimes of molecular relaxation processes. In the step-anneal experiments up to 60 °C, the higher orientation and the availability of localised motions coupled with insignificant chain retraction relaxations enables the smectic regions to build up in coherence and stability without the formation of crystallisation order. In contrast, in the fast drawing experiments, chain retraction and crystallisation can occur before the build up of stable smectic regions.

It is also worth noting that the WAXS meridonal reflection associated with the transient smectic mesophase was only observable in our previous time-resolved drawing experiments at 90 °C, while deforming at the highest draw rate of ~10 s^{-1} [7]. The inability to resolve the mesophase reflection at the slower draw rates does not necessarily preclude the generality of the smectic phase occurring as a transient intermediate state during the formation of the crystalline phase. At slower draw rates, chain retraction and chain relaxation in general are more able to compete with

the mechanical elongation of chains. Crystallisation from an intermediate smectic order would occur more readily so that the lifetime of individual smectic regions would be reduced. A reduction in lifetime would reduce the instantaneous fraction of chains with smectic order during the early stages of crystallisation and hence reduce the ability to detect smectic reflections.

4.4. Development of four-point SAXS pattern

The SAXS results provide information on the evolution of the diffuse scatter associated with the appearance of the oriented crystalline phase. This is particularly pertinent to the time-resolved drawing experiment where the process occurs continuously at constant temperature and where there is quantitative data from the WAXS on the development of crystallinity [2,22]. In the early stages of crystallisation (e.g. frames 9 and 10 in Fig. 1), the diffuse scatter occurs at lower scattering angles giving the impression of a diagonal cross rather than a four-point pattern. With further crystallisation (e.g. frames 11, 12, 20 and 49 of Fig. 1), the pattern expands outwards to produce the final, discrete four-point pattern, which then increases in intensity. The exact nature of the earliest pattern is difficult to discern in the raw data because of the dominance of the intense, central scattering. It can be clarified by subtracting frame 8 from consecutive frames as shown in Fig. 12. This shows that, although the scatter is concentrated along the diagonal direction, the maxima in intensity occur along the arms of the cross.

The concept of microfibrils, referred to above, is often used as a framework for interpreting two-dimensional SAXS patterns of crystalline polymers [19]. Two main approaches have been used to explain the four-point patterns from microfibrils. In one case, it is assumed that the crystals within the fibrils are lamellae with inclined end-faces and that there is no correlation of crystals between neighbouring fibrils. In this model, the diffraction maxima from the long period repeat in the fibril is moved away from the meridional axis by an angle related to the inclination of the lamellae end faces. In the other case, it is proposed that there are correlations between crystals in neighbouring fibrils giving a morphology similar to a three-dimensional chess board. Both models can reproduce the main features of the observed four-point patterns and it is likely that elements of both could be present.

The development of the SAXS pattern should be related to the crystallisation kinetics. Our previous synchrotron WAXS studies of fast drawn PET have shown that the kinetics of the crystallisation process closely follow a first order transformation [22]. We proposed that it is appropriate to interpret these kinetics in terms of a sporadic nucleation of crystals within the extended chain network. Accordingly in the earliest stages of the primary crystallisation such crystallites would be spatially uncorrelated and the very earliest SAXS pattern should therefore be associated with the intensity function of an isolated crystal. As additional crystal nuclei fill in the gaps, correlations between crystals would develop, resulting in the appearance of the intensity function of correlation peaks, which would move outwards with progressive in-filling of crystals.

The earliest SAXS pattern shown in Fig. 12 corresponds to the point where about 25% of the final crystallinity has been achieved. The presence of intensity peaks shows that correlations between crystals are already present at this stage. This could be the consequence of the sporadic crystals being located within fibrillar entities where there is a well defined lateral correlation between fibrils. It would be of interest to know the nature of SAXS at an even earlier stage of the crystallisation process since this could help clarify the nature of individual crystals. Further investigations are therefore planned to resolve the development of the SAXS pattern in more detail. It also worth noting that Fig. 12 shows evidence of a very weak equatorial streak which is similar in character to that seen in Fig. 8 for the step-anneal experiment and which may signify a very small amount of smectic mesophase.

5. Conclusions

The step anneal experiment provides confirmation of the smectic mesophase acting as a precursor state which transforms to the triclinic crystal phase when annealed

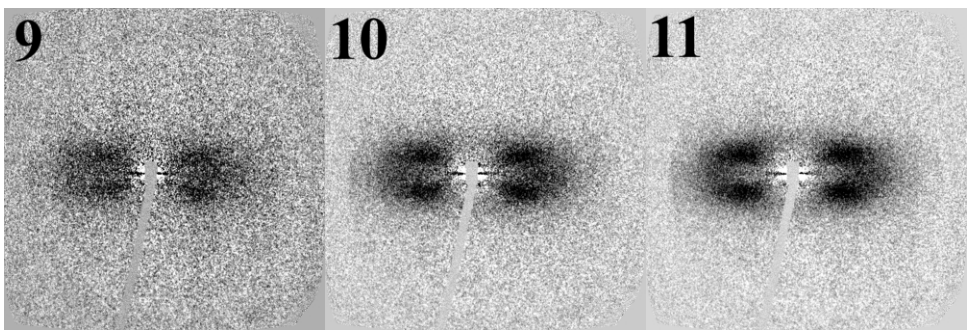

Fig. 12. Early stages of development of four-point SAXS pattern in time-resolved drawing experiment obtained from data in Fig. 1 by subtracting frame 8 from subsequent frames 9, 10 and 11.

between 70 and 100 °C. The SAXS patterns exhibit two components of scatter, comprising equatorial lobes close to the main beam and diffuse scatter at higher angle with a four-point character. The experiment demonstrates that the equatorial scatter is associated with the smectic mesophase. It shows that the smectic domains have a needle-like or columnar morphology where the smectic domains are at least 75 nm long and have an inter-domain separation of around 20 nm. The lateral spread of the WAXS meridional reflection shows that the lateral coherence of the chains in the smectic domains increases from 2 to 4 nm when heated from the 30 °C 'as-drawn' state to the 70 °C annealed state. The diffuse SAXS evolves from a cross-like appearance to a well resolved four-point pattern when annealing between 70 and 100 °C. This scatter is wholly associated with the crystalline phase and correlates quantitatively with the appearance and growth of the crystalline phase.

The time-resolved drawing experiments were restricted to slower draw rates by the limiting time resolution of the SAXS detector. These experiments show a similar development of a four-point SAXS pattern, which correlates quantitatively with the appearance of crystallinity. Although the meridional smectic reflection could not be detected in the WAXS data at these slower draw rates there is evidence of a weak equatorial SAXS data indicating the transient occurence of the smectic mesophase. Differences between experiments in the stability of the smectic phase during the transformation to the crystalline phase can be attributed to different chain relaxation processes available under different conditions.

Acknowledgements

We would like to acknowledge the inspiring discussions with Professor Ian Ward FRS based on his earlier research into the smectic phase of polyesters and his continuous interest in this topic. This work was supported by the allocation of beam time at the ESRF. We are grateful to M.G. Davies, E.J.T. Greasley, and M.P. Wallace for technical support.

References

[1] Blundell DJ, Mahendrasingam A, Martin C, Fuller W, MacKerron DH, Harvie JL, Oldman RJ, Riekel C. Polymer 2000;41:7793.
[2] Mahendrasingam A, Blundell DJ, Martin C, Fuller W, MacKerron DH, Harvie JL, Oldman RJ, Riekel C. Polymer 2000;41:7803.
[3] Keller A. Crystallisation of polymers. In: Dosier M, editor. NATO Advanced Research Workshop. Mons Belgium: Kluwer; 1992. p. 1.
[4] Terril NJ, Fairclough PA, Towns-Andrews E, Komanschek BU, Young RJ, Ryan AJ. Polymer 1998;39:2381.
[5] Ryan AJ, Fairclough PA, Terril NJ, Olmsted PD, Poon WCK. Faraday Discuss 1999;112:13.
[6] Olmsted PD, Poon WCK, McLeish TCB, Terril NJ, Ryan AJ. Phys Rev Lett 1998;81:373.
[7] Mahendrasingam A, Martin C, Fuller W, Blundell DJ, Oldman RJ, MacKerron DH, Harvie JL, Riekel C. Polymer 2000;41:1217.
[8] Auriemma F, Corradini P, De Rosa C, Guerra G, Petroccone V. Macromolelcules 1992;25:2490.
[9] Nicholson TM, Davies GR, Ward IM. Polymer 1994;35:4259.
[10] Windle AH. In: Shibaev VP, Lam L, editors. Liquid crystalline and mesomorphic polymers. New York: Springer; 1994.
[11] Welsh GE, Blundell DJ, Windle AH. Macromolecules 1998;31:7562.
[12] Welsh GE, Blundell DJ, Windle AH. J Mater Sci 2000;35:5225.
[13] Blundell DJ, Mahendrasingam A, Martin C, Fuller W. J Mater Sci 2000;35:5057.
[14] Bonart von R. Kolloid Z Z Polym 1966;213:1.
[15] Bonart von R. Kolloid Z Z Polym 1968;231:16.
[16] Asano T, Seto T. Polym J 1973;5:72.
[17] Asano T, Balta-Calleja FJ, Flores A, Tanigaki M, Mina MF, Sawatari C, Itigaki H, Takahahi H, Hatta I. Polymer 1999;40:6475.
[18] Imai M, Kaji K, Kanaya T. Macromolecules 1994;27:7103.
[19] Balta-Calleja FJ, Vonk CG. X-ray scattering of synthetic polymers. Amsterdam: Elsevier; 1989. Chapter 7.
[20] Mahendrasingam A, Fuller W, Forsyth VT, Oldman RJ, Mackerron DH, Blundell DJ. Rev Sci Instrum 1992;63:1087.
[21] Hughes DJ, Mahendrasingam A, Martin C, Oatway WB, Heeley EL, Bingham SJ, Fuller W. Rev Sci Instrum 1999;70:4051.
[22] Blundell DJ, Mackerron DH, Fuller W, Mahendrasingam A, Martin C, Oldman RJ, Rule RJ, Riekel C. Polymer 1996;37:3303.
[23] Prevorsek DC, Kwon YD, Sharm RK. J Mater Sci 1977;12:2310.
[24] Daubeny R de P, Bunn CW, Brown CJ. Proc R Soc 1954;A226:531.